International Journal of Nanomedicine

Dovepress

open access to scientific and medical research

Open Access Full Text Article

ORIGINAL RESEARCH

Combined Amphiphilic Silybin Meglumine Nanosuspension Effective Against Hepatic Fibrosis in Mice Model

Qin Yang[1,2,*], Tiantian Tan[2,*], Qin He[2], Chenqi Guo[2], Dan Chen[2], Yulu Tan[2], Jiaxing Feng[2], Xu Song[2], Tao Gong[2], Jia Li[3]

[1]School of Pharmacy, North Sichuan Medical College, Nanchong 637100, People's Republic of China; [2]Key Laboratory of Drug-Targeting and Drug Delivery System of the Education Ministry and Sichuan Province, Sichuan Engineering Laboratory for Plant-Sourced Drug and Sichuan Research Center for Drug Precision Industrial Technology, West China School of Pharmacy, Sichuan University, Chengdu 610041, People's Republic of China; [3]West China Hospital of Stomatology, Sichuan University, Chengdu 610041, People's Republic of China

*These authors contributed equally to this work

Correspondence: Jia Li, West China Hospital of Stomatology, Sichuan University, No. 14, Block 3, Southern Renmin Road, Chengdu, 610041, People's Republic of China, Tel +862885503503, Email lijia816@163.com

Introduction: Silybin (SLB) as an effective hepatoprotective phytomedicine has been limited by its hydrophobicity, poor bioavailability and accumulation at lesion sites. Additionally, present drug loading methods are impeded by their low drug loading capacity, potential hazard of materials and poor therapeutic effects. Consequently, there is a pressing need to devise an innovative approach for preparing nanosuspensions loaded with both SLB and Silybin Meglumine salt (SLB-M), as well as to investigate the therapeutic effects of SLB nanosuspensions against hepatic fibrosis.

Methods: The SLB nanosuspension (NS-SLB) was prepared and further modified with a hyaluronic acid–cholesterol conjugate (NS-SLB-HC) to improve the CD44 targeting proficiency of NS-SLB. To validate the accumulation of CD44 and ensure minimal cytotoxicity, cellular uptake and cytotoxicity assessments were carried out for the nanosuspensions. Western blotting was employed to evaluate the anti-hepatic fibrosis efficacy in LX-2 cells by inhibiting the secretion of collagen I. Hepatic fibrosis mouse models were used to further confirm the effectiveness of NS-SLB and NS-SLB-HC against hepatic fibrosis in vivo.

Results: Uniform nanosuspensions were prepared through self-assembly, achieving high drug loading rates of 89.44% and 60.67%, respectively. Both SLB nanosuspensions showed minimal cytotoxicity in cellular environments and mitigated hepatic fibrosis in vitro. NS-SLB-HC was demonstrated to target activated hepatic stellate cells by receptor-ligand interaction between HA and CD44. They can reverse hepatic fibrosis in vivo by downregulating TGF-β and inhibiting the secretion of α-SMA and collagen I.

Conclusion: Designed as a medical excipient analogue, SLB-M was aimed to establish an innovative nanosuspension preparation method, characterized by high drug loading capacity and a notable impact against hepatic fibrosis.

Keywords: nanosuspension, LX-2 cells, phytomedicines, surfactant, drug delivery system

Introduction

Hepatic fibrosis is a defining feature of almost all types of chronic liver disease[1] and its development has been associated with the activation of hepatic stellate cells (HSCs).[2,3] Under pathological conditions, HSCs become activated and differentiate into myofibroblast-like cells that deposit extracellular matrix (ECM),[4,5] promoting hepatic fibrosis. Although HSCs are protected in the Disse space, small drug particles (<100 nm) can reach them by passing through the holes on the surface of adjacent liver sinusoidal endothelial cells, allowing the drug to reverse HSC activation.[3,5–7] The CD44 receptor is expressed on the surface of activated HSCs to a much greater extent than on the surface of quiescent HSCs, suggesting that CD44-targeting nano-formulations should be particularly effective against hepatic fibrosis.[2,8]

Received: 8 June 2023
Accepted: 6 September 2023
Published: 12 September 2023

There are many compounds that can alleviate hepatic fibrosis in vitro, such as curcumin and silybin. However, these substances show weak activity in vivo due to their high hydrophobicity, rapid clearance, and poor targeting capabilities.[9,10] To overcome these limitations, nanopreparation strategies have been applied to formulate these compounds into liposomes, nano-emulsions, inclusion compounds, and nanoparticles.[11–13] Alya, et al[14] made significant efforts to load curcumin into silver nanoparticles, which showed satisfying anti-liver fibrosis activity and confirmed the fact that nanopreparations have a size benefit against liver fibrosis. Li, et al[3] reported a nanomicelle strategy to load silybin, which showed significant liver targeting effect. However, the drug loading capacity was less than 7%, which limits their clinical use due to the large amounts of surfactants and induce severe side effects such as hemolysis, adverse reactions, and respiratory system dysfunction.[15]

Surfactants are commonly used to improve the encapsulation and performance of drugs,[16,17] as they consist of a hydrophobic and a hydrophilic part, which make them suitable wetting agents, emulsifiers, and solubilizers.[18] However, due to the large amount needed and the risk of safety, few of them can be applied in preparations for intravenous injection.[19] Next-generation surfactants, such as polymeric supra-amphiphiles,[20] surfactant-like amphiphilic conjugates,[21] and prodrugs[22] have been developed, but their preparation requires toxic reagents such as irinotecan and mitoxantrone derivatives.[22,23]

As is well known, silybin (SLB) is extracted from the fruits and seeds of milk thistle and has attracted attention due to its safety, as well as its anti-cancer,[24] anti-inflammatory, hepatoprotective, and cardioprotective activities.[25,26] Silybin meglumine salt (SLB-M), a meglumine salt of SLB has shown minimal cytotoxicity at concentrations below 60 μM.[27] We wondered whether, SLB-M can engage in stronger π–π stacking interactions with SLB and other hydrophobic drugs than the stacking interactions between hydrophobic drugs and traditional surfactants.[3,15] If yes, SLB-M might be a safe and effective surfactant in the manufacture of hydrophobic drug delivery systems.

In this study, we used SLB-M to construct a minimal-carrier drug loading system with high drug loading efficiency, safety, and efficacy against hepatic fibrosis. In this system, SLB-M and SLB were self-assembled through π–π stacking[22,23] to give a uniform nanosuspension of ~30 nm (NS-SLB), which we showed to accumulate in the liver, pass through the Disse barrier, and reach activated HSCs. NS-SLB also escaped clearance by the mononuclear phagocyte system due to its small size,[28,29] and it effectively targeted activated HSCs. To further increase its therapeutic effect, NS-SLB was modified with a hyaluronic acid–cholesterol conjugate, and the resulting NS-SLB-HC targeted activated HSCs through recognition of the hyaluronic acid receptor CD44.[4]

Materials and Methods

SLB was purchased from Meilunbio® (Dalian, China). Sodium hyaluronate was purchased from Freda (Shandong, China). *N*-methyl-*D*-glucamine and cholesterol chloroformate (CHO-Cl) were purchased from Best-reagent (Chengdu, China). 1-hydroxy-2,5-pyrrolidinedione (NHS), 1,2-ethylenediamine, 1-hydroxybenzotriazole (HOBT) and 1-ethyl-3-(3-dimethylaminopropyl) carbodiimide (EDC) were purchased from Kelong (Chengdu, China). 1,1′-dioctadecyl -3,3,3′,3′-tetramethylindodicarbocyanine perchlorate (DiD) was purchased from J&K® (Beijing, China). CD44 monoclonal antibody labeled with R-phycoterythrin (PE) for flow cytometry, bicinchoninic acid (BCA) protein assay kit, transforming growth factor (TGF) β-1 mouse enzyme-linked immunosorbent assay (ELISA) kit, and fluorophore-conjugated antibodies were purchased from Thermo Fisher Scientific (San Diego, USA). Other chemical reagents obtained commercially were of analytical grade or better.

Kunming mice were purchased from the Experimental Animal Center of Sichuan University (Chengdu, China) and kept under specific pathogen-free (SPF) conditions. All animal experiments were approved by the Institutional Animal Care and Ethics Committee of Sichuan University in accordance with the Chinese Guidelines for the Care and Use of Laboratory Animals (SYXK(川)2018–113).

The Preparation of Silybin Meglumine

The silybin meglumine[3] was prepared as the following processes: SLB (0.20 g, 0.41 mmol) was added to anhydrous ethanol (5 mL) and refluxed at 80°C. After the solution turned transparent, meglumine (0.12 g, 0.61 mmol) dissolved in deionized (DI) water (1 mL) was added to the SLB solution, and the reaction was stirred at 80°C for another 10 minutes. The reaction

solution was then preserved at −20°C for 8 hours, and the sediment was collected by centrifuging at 12,000 rpm for 10 minutes. After washing twice with anhydrous ethanol, centrifuging and desiccation, the resulting mustard powder SLB-M was obtained. It can be dissolved well in water and was used as the free SLB solution in later experiments.

The Preparation of Silybin Nanosuspension with Silybin Meglumine

The prepared SLB-M was designed as a solubilizer for an amphiphilic structure to formulate the NS-SLB nanosuspension. SLB-M (8 mg) and SLB (40 mg) were dissolved in dimethylsulfoxide (DMSO, 1 mL). Then, the DMSO solution was added to a 5% ice-cold aqueous solution of saccharose (40 mL). After being freeze-dried, a yellowish oily NS-SLB nanosuspension was obtained. It could be dispersed in a 0.075% aqueous solution of povidone (PVP, K30) or water for injection when needed.

The Preparation of CD44 Targeting Nanosuspension with Hyaluronic Acid-Cholesterol Conjugate

Hyaluronic acid-cholesterol (HC) conjugate was obtained using previously reported methods, and details can be found in Figure S1.[30] HC (15 mg), PVP (30 mg) and saccharose (900 mg) were mixed and dispersed uniformly in DI water (30 mL) by probe ultrasonography. SLB-M (15 mg) and SLB (30 mg) were dissolved in 1 mL of DMSO. The DMSO solution was added dropwise to the above aqueous solution. The resulting mixture was homogenized by probe ultrasonography (100 W, 3 minutes) and then lyophilized. The yellowish flake solid NS-SLB-HC was obtained and could be dispersed in water for injection when needed.

To prepare DiD-loaded nanosuspensions, the pure DMSO was replaced with DiD-DMSO solution, and the resulting solutions were marked as NS-SLB-DiD and NS-SLB-HC-DiD, respectively, both with a concentration of 5 μg/mL. The same protocol was used for the preparation of both nanosuspensions.

The Characterization of Nanosuspensions

The particle size and zeta potential of the nanosuspension were measured using dynamic light scattering (DLS) (Zetasizer Nano ZS90, Malvern, UK) at 25°C. The size variation trend of nanosuspension kept at 4°C was monitored using DLS over 14 days. The morphology of the nanosuspension was observed using transmission electron microscopy (TEM) (H-600 TEM, Hitachi, Japan) with negative staining using 2% phosphotungstic acid. The ultraviolet-visible (UV-vis) absorbance spectra of free SLB, SLB-M, NS-SLB and NS-SLB-HC dissolved in DI water were obtained within a wavelength range of 200–500 nm using a UV-vis spectrophotometer (UV-2600I, Shimadzu, Japan). The encapsulation efficiency (EE) was studied with sephadex G-50 in separating nanoparticles from nanosuspensions and determined using high performance liquid chromatography (HPLC) (UltiMate® 3000, Thermo Scientific, USA). While drug loading efficiency (LE) of SLB were determined using HPLC, calculated using the following equation.[31]

$$EE\ (\%, w/w) = W_{entrapped\ SLB} / W_{fed\ SLB} \times 100\%$$

$$LE\ (\%, w/w) = W_{loaded\ SLB} / W_{nanosuspension} \times 100\%.$$

Cell Lines and Cultures

The human hepatoma cells ($HepG_2$), human hepatocytes (LO_2), and mouse macrophages ($RAW_{264.7}$) were obtained from the cell bank at the Chinese Academy of Science (Shanghai, China). The human hepatic stellate cells (LX-2), can be used as activated HSC cells in vitro under serum activation,[7,32–34] were kindly provided by the State Key Laboratory of Biotherapy, Sichuan University (Chengdu, China).

$HepG_2$, LO_2, and immortalized LX-2 cells were cultured in Dulbecco's modified Eagle's medium (DMEM), and $RAW_{264.7}$ cells were cultured in complete Roswell Park Memorial Institute 1640 (RPMI-1640) in a humidified atmosphere of 5% CO_2 at 37°C. The culture medium mentioned above was supplemented with 10% fetal bovine serum (FBS) and 1% penicillin-streptomycin combination.

The Cellular Uptake of Nanosuspensions in vitro

LX-2 ($CD44^+$), $HepG_2$ ($CD44^+$), LO_2 ($CD44^-$), and $RAW_{264.7}$ ($CD44^-$) cells were seeded in 12-well plates at a density of 1×10^5 cells per well and incubated for 12 hours, under a humidified atmosphere of 5% CO_2 at 37°C. The culture medium was replaced with 1 mL of medium containing DiD solution, NS-SLB-DiD, and NS-SLB-HC-DiD, respectively (0.5 μg/mL DiD dissolved in 1% DMSO). The cells were incubated for 2 hours and washed three times with cold phosphate-buffered solution (PBS). Then, the cells were resuspended, washed three times, and obtained by centrifuging at 2000 rpm for 3 minutes. Next, the centrifuged cells were resuspended in 0.5 mL of PBS and the fluorescent intensity was measured by flow cytometer (Cytomic^{TM} FC 500, Beckman Coulter, USA). To confirm that CD44 receptors mediated the uptake of particles, CD44 receptors on the cells were blocked with 10 mg/mL HA for 4 hours. Then, the cells were exposed to DiD solution, NS-SLB-DiD and NS-SLB-HC-DiD for 2 hours, washed and resuspended in PBS for analysis.

The Cytotoxicity of Nanosupensions

The cytotoxicity was determined using the 3-(4,5-dimethylthiazol-2-thiazolyl)-2,5-diphenyltetrazolium bromide (MTT) assay. Briefly, cells were seeded in 96-well plates at a density of 5000 cells per well and incubated for 12 hours. The medium was then replaced with 100 μL of medium containing serial dilutions of SLB, NS-SLB, NS-SLB-HC, and excipient solutions (the concentration of SLB ranged from 1.0 μg/mL to 50 μg/mL) for 48 hours. Next, 100 μL of MTT solution (0.5 μg/mL in PBS) was added into each well, and the cells were incubated for 4 hours at 37°C. Then, the medium was discarded, and 100 μL of DMSO was added to dissolve the formed formazan crystals. The absorbance at 490 nm was recorded using a microplate reader (Tecan spark 10M, China). Cell viability (%) was calculated according to the following equation:

$$\text{Cell viability}(\%)=\frac{A_{test}-A_{blank}}{A_{control}-A_{blank}}\times100\%$$

The Inhibition of Collagen I Secretion in vitro

The anti-hepatic fibrosis efficacy was evaluated by western blotting in vitro. LX-2 cells were seeded in 12-well plates at a density of 1×10^5 cells per well and incubated for 12 hours. The medium was then replaced with SLB, NS-SLB, NS-SLB-HC, and excipient solutions (the concentration of SLB was set at 20 μg/mL) for 24 hours. Cells were collected and lysed with lysis buffer supplemented with a protease inhibitor in an ice water bath for 30 minutes. The concentration of the lysate was measured using a BCA Kit. Sample buffer was added to the lysate (V: V = 4:1) and boiled for 5 minutes. Lysed samples with a protein concentration of 20 μg were separated by sodium dodecyl sulfate-polyacrylamide gel electrophoresis (SDS-PAGE) and transferred to a polyvinylidene difluoride membrane (1620177, Bio Rad, USA). The membrane was then incubated in 5% fat-free milk prepared with Tris-buffered saline containing 0.1% Tween-20 (TBST) to block the non-specific binding for 1 hour. The membrane was subsequently incubated with primary antibody (anti-collagen I antibody, 1:1000, ab88147, Abcam, UK) at 4°C overnight. Finally, the membrane was incubated with a horseradish peroxidase-conjugated secondary antibody for 1 hour and detected using a Bio-Rad ChemiDoc MP System (Bio-Rad Laboratories, USA).

The Establishment of Hepatic Fibrosis Mouse Models

Mice were subjected to treatment with 2 mL/kg body weight of CCl_4, which had been diluted 4 times in soybean oil. This treatment was administered via intraperitoneal injection twice weekly for a duration of 8 weeks, aiming to induce a liver fibrosis model associated with CCl_4 intoxication.

Mice were anesthetized with chloral hydrate and underwent midline laparotomy. The common bile duct was ligated with silk sutures. After the procedure, the abdomen was closed, and a sham operation was performed without ligating the bile duct to create a liver fibrosis model involving bile duct ligation, marked as the BDL model.[35]

The Distribution of Nanosuspensions in vivo

Normal mice were randomly divided into three groups (n = 15) and intravenously injected with SLB, NS-SLB or NS-SLB-HC at a dosage of 8 mg/kg SLB. Mice were sacrificed at 0.5, 1 and 2 hours after injection. Major organs (heart, liver, spleen, lung, and kidney) were excised, washed with saline solution, dried with filter paper, weighed, and homogenized with double volume of PBS (mL/g). Methanol was added and the homogenate was eddied for 5 minutes (V: V = 4:1). The supernatant was obtained by centrifuging at 13,500 rpm for 5 minutes and detected by HPLC.

Liver fibrosis mice induced by CCl_4 injection were divided into three groups (n = 15) to study the distribution behavior of SLB nanosuspension under pathological conditions. The subsequent steps were as described above.

To intuitively investigate the distribution of SLB nanosuspension, immunofluorescence was applied. CCl_4 -induced liver fibrosis mice were randomly divided into three groups (n = 5) and intravenously injected with DiD, NS-SLB-DiD or NS-SLB -HC-DiD at a dosage of 10 μg/kg DiD, and were sacrificed at 30 minutes after injection. Liver tissues were collected and frozen sections (8 μm) were prepared using a cryostat microtome (Leica, CM960, Germany). The secreted collagen I and highly expressed CD44 were set as markers of fibrotic liver, and were respectively stained as described below.

Sections were fixed in 4% paraformaldehyde for 5 minutes at 4°C, washed three times with PBS for 3 minutes, and then incubated with 0.5% triton X-100 for 5 minutes. Next, the sections were washed twice with PBS, blocked with serum buffer for 1 hour and incubated with relevant primary antibodies (anti-CD44 antibody: ab189524, Abcam, UK; anti-collagen I antibody: ab34710, Abcam, UK) diluted in blocking buffer for 12 hours at 4°C. After three washes with PBS, the sections were incubated with the secondary antibody (Alexa Fluor® 488, diluted in PBS) for 1 hour. Following three rinses with PBS, the nuclei were stained with 2-(4-amidinophenyl)-6-indolecarbamidine dihydrochloride (DAPI) stain solution for 5 minutes. Finally, the sections were observed using CLSM.

Efficacy of Nanosuspensions Against Hepatic Fibrosis and Systemic Toxicity in vivo

The efficacy of hepatic fibrosis treatment and the assessment of systemic toxicity were evaluated in vivo using two animal models: BDL and CCl_4 mouse. Hepatic fibrosis mice were randomly divided into four groups (n = 10): normal saline group (Saline), SLB solution group (SLB), SLB nanosuspension group (NS-SLB), and HC-modified SLB nanosuspension group (NS-SLB-HC), at a dosage of 8 mg/kg SLB twice a week via the tail vein.

For the CCl_4 model, treatment started after 8 weeks of i.p. injection of CCl_4. Healthy mice (n = 10) were included without any treatment (Normal). Mice were sacrificed (n = 5) at the 10th and 12th weeks respectively, and tissues and serum were collected. The appearance and histological analysis (H&E and Masson stain) of the liver were applied to evaluate the progression of liver fibrosis. The concentration of aspartate transaminase (AST) and alanine transaminase (ALT), key indexes of pathological liver, were detected using an automatic biochemical analyzer (Cobas C 311, Roche Diagnostics, Germany). The concentration of TGF-β, which stimulates the activation of HSCs, was detected according to the protocol of the ELISA kit (TGF β-1/LAP mouse uncoated ELISA kit, 88-50,690-22, Thermo Fisher Scientific, USA).

For the BDL-induced model, treatment began on the 3rd day after operation, and a sham group (n = 10) was included without bile duct ligation and treatment (Control). Mice were sacrificed (n = 5) at the 2nd and 3rd weeks respectively. The appearance, histological analysis, ALT, AST, and TGF-β were evaluated as described previously. The H&E analysis of other tissues were conducted to evaluate the toxicity of the nanosuspension.

For immunohistochemical analysis, stretchy fiber (α-smooth muscle actin, α-SMA) and collagen I stain were applied to further evaluate the anti-hepatic fibrosis efficacy. To label the α-SMA overexpressed by activated HSCs under pathological conditions[29,36], sections were stained with a mouse anti-alpha SMA antibody (1:400, diluted with 2% goat serum, ab7817, Abcam, U.K.). And sections were incubated with a 488-labeled goat anti-mouse secondary antibody (1:500, diluted with PBS, A-11001, Thermo Fisher Scientific, USA).

Statistical Analysis

The statistical analysis was conducted using either a student's *t*-test or a one-way analysis of variance (ANOVA) with Graphpad Prism software. All experiments were repeated at least three times. The data were expressed as mean ± standard deviations (S.D.). Statistical significance was set at a P value less than 0.05.

Results

Characterization of NS-SLB and NS-SLB-HC

NS-SLB and NS-SLB-HC were prepared using the freeze-drying method, and transmission electron microscopy analysis revealed that both formulations were spheroidal and had a narrow size distribution. The average particle size of NS-SLB was 37.9 ± 7.2 nm, with a polydispersity index (PDI) of 0.233 ± 0.038, and an average zeta potential of −17.6 ± 1.1 mV (as shown in Figure 1). After modification, the nanoparticle size increased to about 87 nm, with a PDI of 0.170 ± 0.043

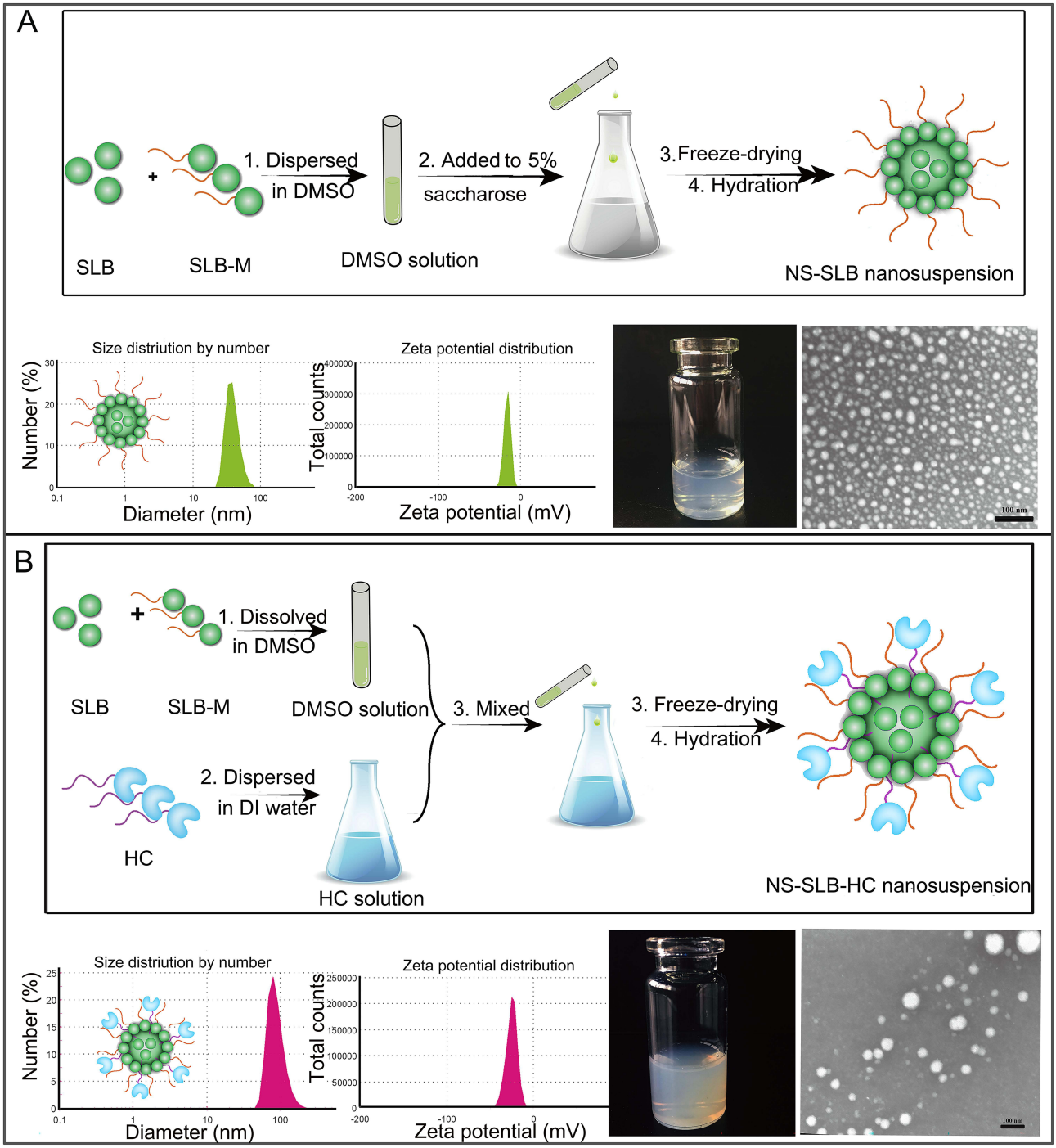

Figure 1 Preparation, dynamic light scattering measurements, photographs in solution, and transmission electron micrographs of (**A**) NS-SLB and (**B**) NS-SLB-HC. Scale bar, 100 nm.

and a zeta potential of −23.3 ± 2.2 mV. Both nanosuspensions exhibited strong size stability under dispersed conditions, with minimal size growth of less than 5 nm observed over a 2-week period (Figure S2). As shown in Figure S3, hydrophobic SLB is hardly dissolved in DI water, so the saturated SLB solution shows the lowest UV-vis absorbance compared with SLB-M solution and nanosuspensions. In accordance with reported trends, when SLB-M was loaded into nanosuspensions, there was an obvious change in absorption, with two maximum absorption peaks of SLB-M and nanosuspensions (around 326 nm and 286 nm). The ration of the two maximum absorptions of SLB-M was about 1.56. However the values of NS-SLB and SN-SLB-HC decreased to 0.87 and 1.03, respectively, owing to the π-π stacking between the hydrophobic flavonoid structure of SLB and SLB-M, which formed nanosuspensions.[22] SLB encapsulation efficiency was over 80% (Table 1), indicating successful loading of the hydrophobic drug. Moreover, the loading efficiency was above 60%, which was significantly higher than the 6.9 ± 0.3% we achieved before.[3]

Cellular Uptake of NS-SLB and NS-SLB-HC in vitro

To investigate the cellular internalization of the prepared formulations, NS-SLB and NS-SLB-HC were labeled with DiD, which is a hydrophobic cell membrane staining agent, and incubated with CD44-overexpressing cells (LX-2 and $HepG_2$) or CD44-underexpressing cells (LO_2 and $RAW_{264.7}$) (Figure S4). We found that LX-2 and $HepG_2$ cells took up NS-SLB-HC-DiD significantly more than they took up NS-SLB-DiD (Figure 2A). This indicates that the modification with hyaluronic acid enhanced the nanosuspension's ability to target CD44, which is consistent with our previous findings.[3,6] Furthermore, the $RAW_{264.7}$ cells took up NS-SLB-DiD to a similar extent as other cell types probably because of the nano-size and the outer meglumine layer, which can form a hydration shell similar to the stealth PEG-hydrated layer, thus protecting the nanosuspensions from being phagocytosed by macrophages.3.3 Cytotoxicity of NS-SLB and NS-SLB-HC.

Previous studies have indicated that SLB is weakly toxic to LX-2 cells, $HepG_2$ cells, and human skin fibroblasts at concentrations below 60 μM (~28.9 μg/mL).[27] Our findings are consistent with these results, as we observed that even at concentrations up to 50 μg/mL, SLB displayed low toxicity against LX-2, $HepG_2$, LO_2 and $RAW_{264.7}$ cells, with cell viability being 65% of the level in untreated control cells (Figure 2B). These results suggest that SLB exhibits minimal cytotoxicity, indicating that NS-SLB may be a suitable option for treating hepatic fibrosis.

Inhibition of Collagen I Secretion in vitro

The activation of HSCs in hepatic fibrosis leads to the secretion of excessive amounts of collagen I.[6,10] To examine the effect of the prepared nanosuspensions on collagen secretion in activated HSCs, Western blotting was used to measure the levels of collagen in LX-2 cells treated with different formulations for 24 hours (Figure 2C and D). Free SLB (20 μg/mL) reduced collagen secretion to 64.14% of the level in untreated LX-2 cells, possibly due to its ability to inhibit Smad2/3-dependent signaling, which helps drive hepatic fibrosis.[12] Moreover, Collagen I secretion was even more strongly inhibited by NS-SLB and NS-SLB-HC, suggesting that both formulations mitigate hepatic fibrosis in vitro.

Establishment of Mouse Models of Hepatic Fibrosis

The successful construction of mouse models with CCl_4- or BDL-induced liver fibrosis was visually confirmed and through staining of liver sections with H&E and Masson staining. Normal liver appeared bright red with a shiny surface and soft texture, whereas fibrotic livers were dull or light red, with a rough surface and firm texture (Figure S5). The two fibrotic models also showed excessive deposition of ECM, collagen accretion, and destruction of hepatic lobules and pseudolobules.

Table 1 The Encapsulation Efficiency (EE) and Drug Loading Efficiency (LE) of SLB Nanosuspension, n = 3

Groups	NS-SLB	NS-SLB-HC	NS-SLB-DiD	NS-SLB-HC- DiD
EE (%)	85.60 ± 2.88	90.83 ± 1.39	85.07 ± 4.88	89.37 ± 3.37
LE (%)	89.44 ± 3.94	60.67 ± 3.75	/	/

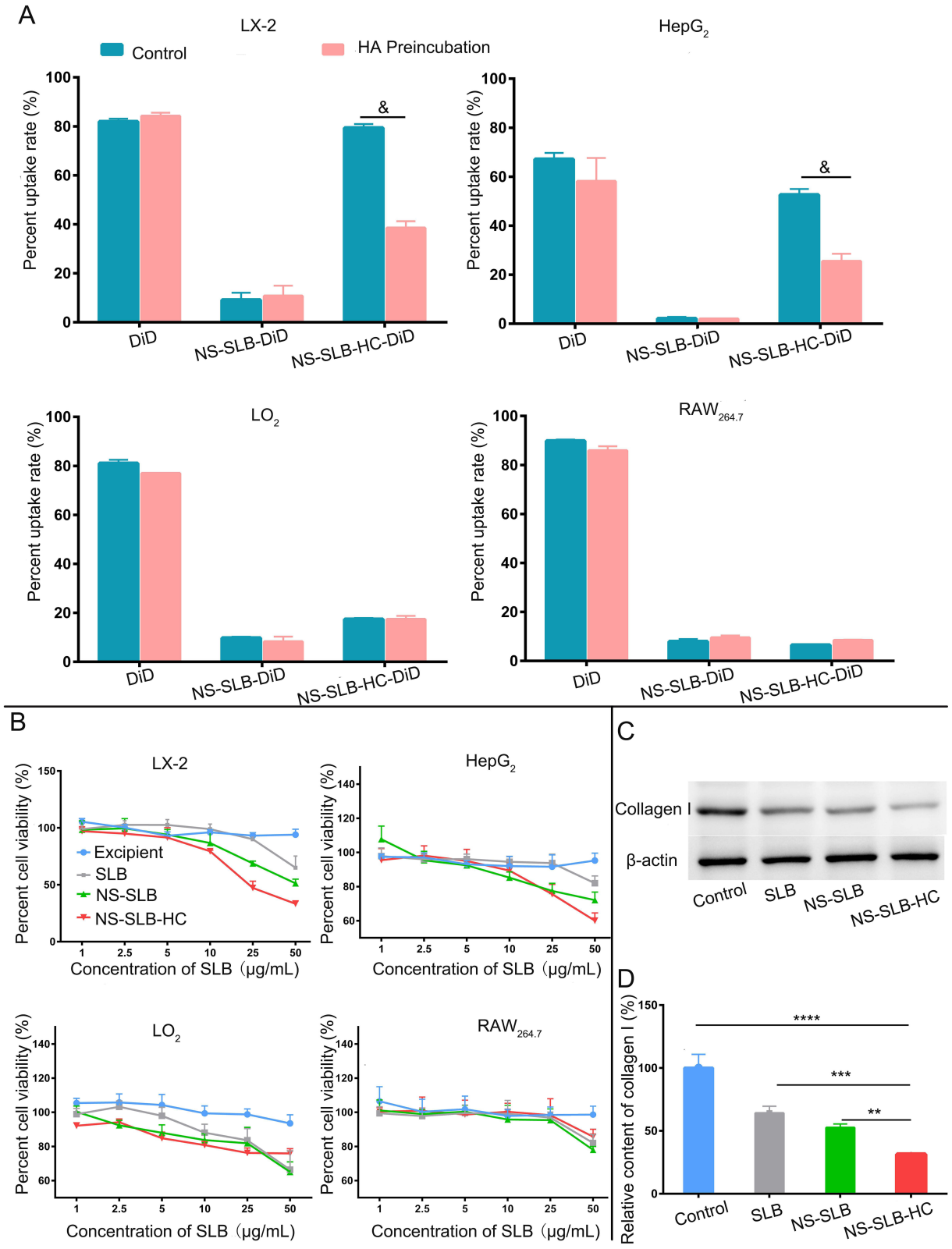

Figure 2 Cellular uptake, cytotoxicity, and inhibition of collagen I secretion in vitro. (**A**) Cellular uptake of free DiD, NS-SLB-DiD, and NS-SLB-HC-DiD by LX-2, $HepG_2$, LO_2, and $RAW_{264.7}$ cells, as detected by flow cytometry after 2 h of treatment. Control, cells treated with free SLB or SLB nanosuspensions; HA preincubation, cells treated with nanosuspension and hyaluronic acid solution (10 mg/mL, n = 5). The difference analysis was conducted using a student's *t*-test here. $^{\&}P < 0.05$. (**B**) Cytotoxicity of free SLB, NS-SLB, and NS-SLB-HC in LX-2, $HepG_2$, LO_2 and $RAW_{264.7}$ cells after 48-h incubation (n = 5). (**C**) Representative Western blots against collagen I (n = 3). (**D**) Relative content of collagen I in LX-2 cells treated with different formulations (n = 3). Data are shown as mean ± SD. $^{****}P < 0.0001$; $^{***}P < 0.001$; $^{**}P < 0.01$.

Distribution of Nanosuspensions in vivo

To explore the biodistribution of the prepared nanosuspensions, we measured the concentration of SLB in liver tissues from control mice and mice with CCl_4-induced fibrosis that received different preparations (Figure 3A and S6). In normal mice, free SLB was mainly distributed to the kidneys and lungs, and little was detected in the liver after 60 minutes, indicating rapid metabolism of SLB. In contrast, NS-SLB and NS-SLB-HC were detected mainly in the liver, with NS-SLB-HC showing significantly higher accumulation 60 minutes post-injection, presumably reflecting CD44-mediated endocytosis as previously observed.[3,6] A similar trend was also observed in fibrotic mice.

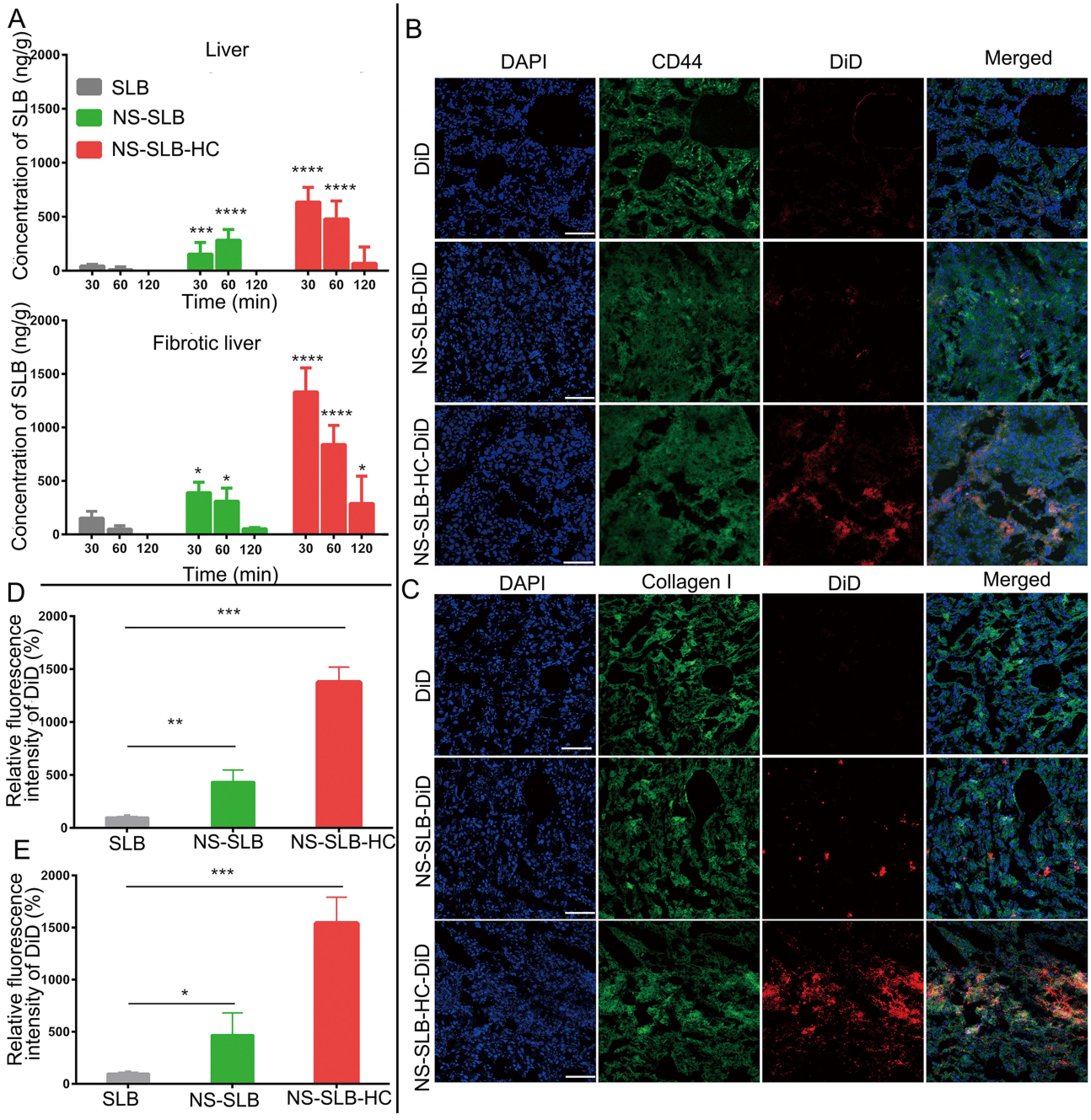

Figure 3 In vivo distribution of SLB, NS-SLB, and NS-SLB-HC. (**A**) Concentration of SLB in normal and CCl_4-induced fibrotic liver tissues. Data are shown as mean ± SD (n = 5). (**B, C**) Biodistribution of different formulations, as determined by immunofluorescence staining against (B) CD44 or (C) collagen I in fibrotic liver tissues with Alexa Fluor® 488-labeled IgG (green). Cell nuclei were stained with DAPI (blue). Scale bar, 50 μm. (**D, E**) Semi-quantitative analysis of immunofluorescence images. Data are shown as mean ± SD (n = 3). ****$P < 0.0001$; ***$P < 0.001$; **$P < 0.01$; *$P < 0.05$ vs free SLB.

Immunofluorescence staining against CD44 and collagen I in fibrotic liver tissues with Alexa Fluor® 488 showed that NS-SLB-DiD accumulated significantly more in the liver than free DiD, and NS-SLB-HC-DiD showed the greatest accumulation of all (Figure 3B-E). These results confirm that the nanosuspensions improve SLB accumulation in the liver, where they facilitate drug passage through the Disse space.

Efficacy Against Hepatic Fibrosis and Systemic Toxicity in vivo

To investigate the efficacy of the prepared formulations against hepatic fibrosis in vivo, mice with CCl_4- or BDL-induced fibrosis were treated with different SLB preparations (Figure 4A and A). In both models, treatment with saline or free SLB resulted in yellow-brown livers with progressive fibrosis and cirrhosis, indicating that cholestasis or continuous intraperitoneal injection of CCl_4 can exacerbate fibrosis (Figures 4B, 5B, S8 and S9). Extensive fibrosis, destroyed liver lobules, as well as square and round pseudolobules were also observed in the saline- and SLB-treated groups, along with the growing fibers. In contrast, livers from animals treated with NS-SLB or NS-SLB-HC showed similar appearance and texture to those of control animals. H&E and Masson staining revealed that the developed formulations exerted strong anti-fibrotic effects, by reducing deposition of collagen fibers and ECM along the central venous or portal area.

Fibrotic mice treated with saline or free SLB showed little weight gain over time (Figure S6A and B), and their ALT and AST levels were significantly higher than those of control mice, indicating severe liver damage (Figures 4C, D, 5C and D). In contrast, mice treated with NS-SLB and NS-SLB-HC steadily gained weight, while ALT and AST levels were only slightly increased. These results were consistent with the in vitro results, confirming that the targeted delivery of SLB to activated HSCs using the developed nanosuspensions can significantly improve therapeutic efficacy.

Previous studies have shown that activated HSCs can upregulate α-SMA and ECM proteins, such as collagen,[9,29] suggesting that the expression levels of these proteins can serve as markers of the degree of fibrosis. Immunofluorescent staining of liver sections against α-SMA and collagen I showed that NS-SLB and NS-SLB-HC significantly down-regulated both proteins compared to saline or SLB (Figure 4E, F, 5E and F). These findings further support that both nanosuspensions can prevent hepatic fibrosis by reversing HSC activation as well as inhibiting secretion of α-SMA and deposition of ECM.

TGF-β is a pro-fibrotic cytokine that plays a key role in the activation of quiescent HSCs,[37,38] and its level may also indicate the degree of fibrosis. SLB suppresses Smad2/3 phosphorylation, thus downregulating TGF-β in plasma.[37,39] In our mouse model, saline or free SLB upregulated TGF-β to a much greater extent than NS-SLB or NS-SLB-HC did (Figure S7). This result may be attributed to the greater efficacy of SLB when delivered in the nanosuspensions. These results suggest that SLB nanosuspensions may reverse HSC activation not only by inhibiting the secretion of α-SMA and collagen I, but also by reducing the expression of TGF-β.

To further investigate the safety of the described nanosuspensions for in vivo applications, we examined their toxicity in major organs. The heart, spleen, and kidneys in the saline and free SLB groups exhibited noticeable pathological changes, such as atrophy of myocardial fibers, disappearance of lymph nodes in the spleen, and a significant decrease in glomerular count (as shown in Figure S10). In contrast, the same organs showed no apparent pathological changes in animals treated with SLB nano-formulations. This may be due to the lower levels of free radicals and selective inhibition of leukotriene production.[40] Therefore, NS-SLB and NS-SLB-HC have the potential to protect key organs from pathological damage without causing any significant toxicity.

Discussion

In this study, we utilized the amphiphilic SLB-M salt as a surfactant to create a minimal-carrier drug loading system for targeted delivery of SLB to activated HSCs for the first time. NS-SLB was formed through π–π stacking interactions between SLB and SLB-M. To improve the CD44 targeting ability and therapeutic efficacy of NS-SLB, we further modified the nanosuspension with a hyaluronic acid–cholesterol conjugate, which is recognized by CD44 on the surface of activated HSCs. Both NS-SLB and NS-SLB-HC demonstrated high encapsulation and drug loading efficiency, as well as good efficacy against hepatic fibrosis. Moreover, both formulations proved to be safe in vitro and in mice. It is well known that the morphological characteristics of particles, including size, shape, surface potential and chemistry,

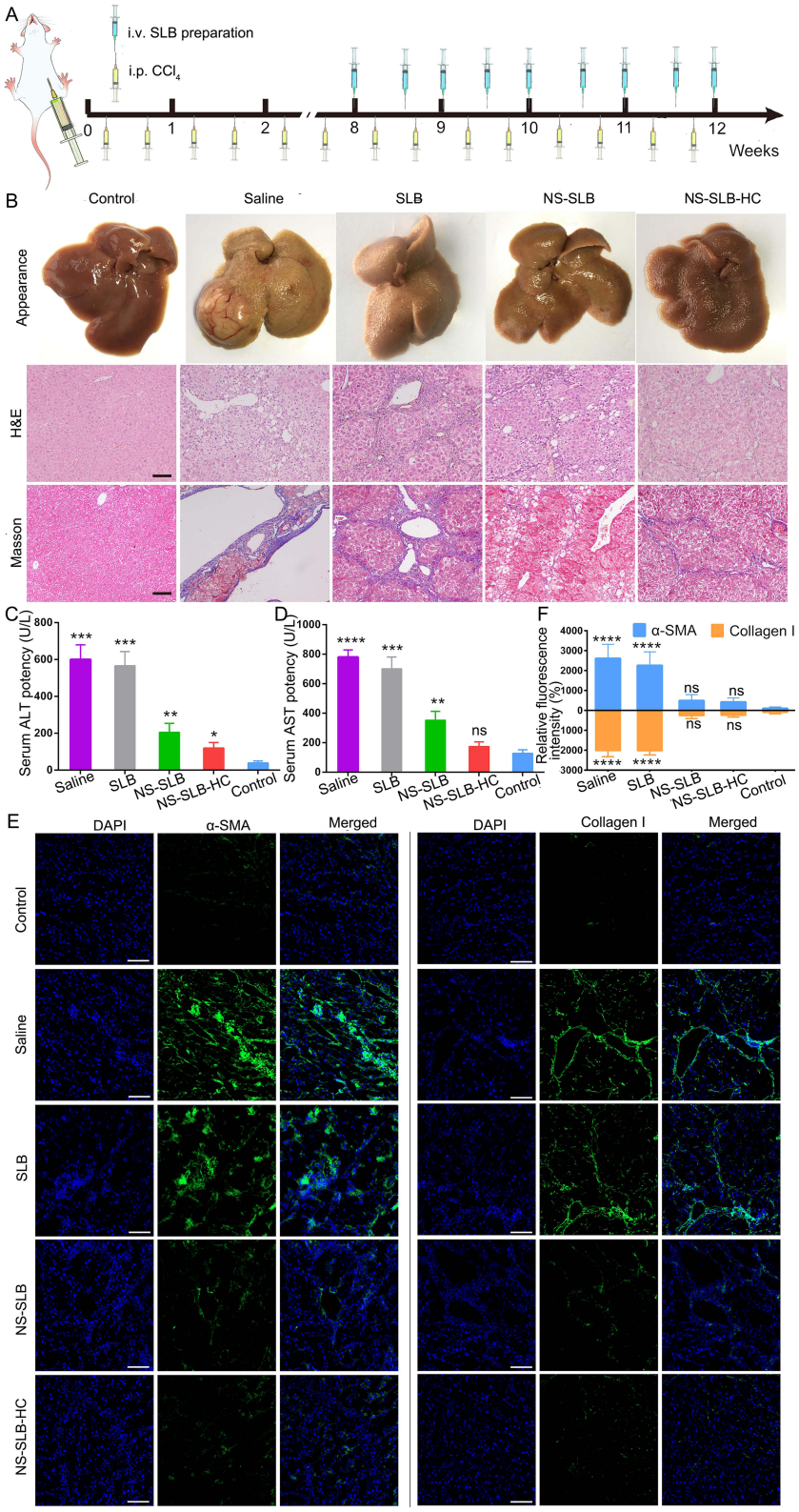

Figure 4 Efficacy of nanosuspensions against CCl_4-induced hepatic fibrosis in mice. (**A**) Schematic of treatment schedule. (**B**) Appearance and histological analysis of liver tissues after 12 weeks of treatment with different formulations. Scale bar, 100 μm. (**C** and **D**) Levels of (C) alanine aminotransferase (ALT) and (D) aspartate aminotransferase (AST) after 12 weeks of treatment. Normal mice were used as controls. (**E**) Immunofluorescence staining of liver sections against α-smooth muscle actin (α-SMA) or collagen I with Alexa Fluor® 488-labeled IgG (green) after 12 weeks of treatment. Cell nuclei were stained with DAPI (blue). Scale bar, 50 μm. (**F**) Semi-quantitative analysis of immunofluorescence images. Data are shown as mean ± SD (n = 5). ****$P < 0.0001$; ***$P < 0.001$; **$P < 0.01$; *$P < 0.05$; ns, non-significant difference vs control.

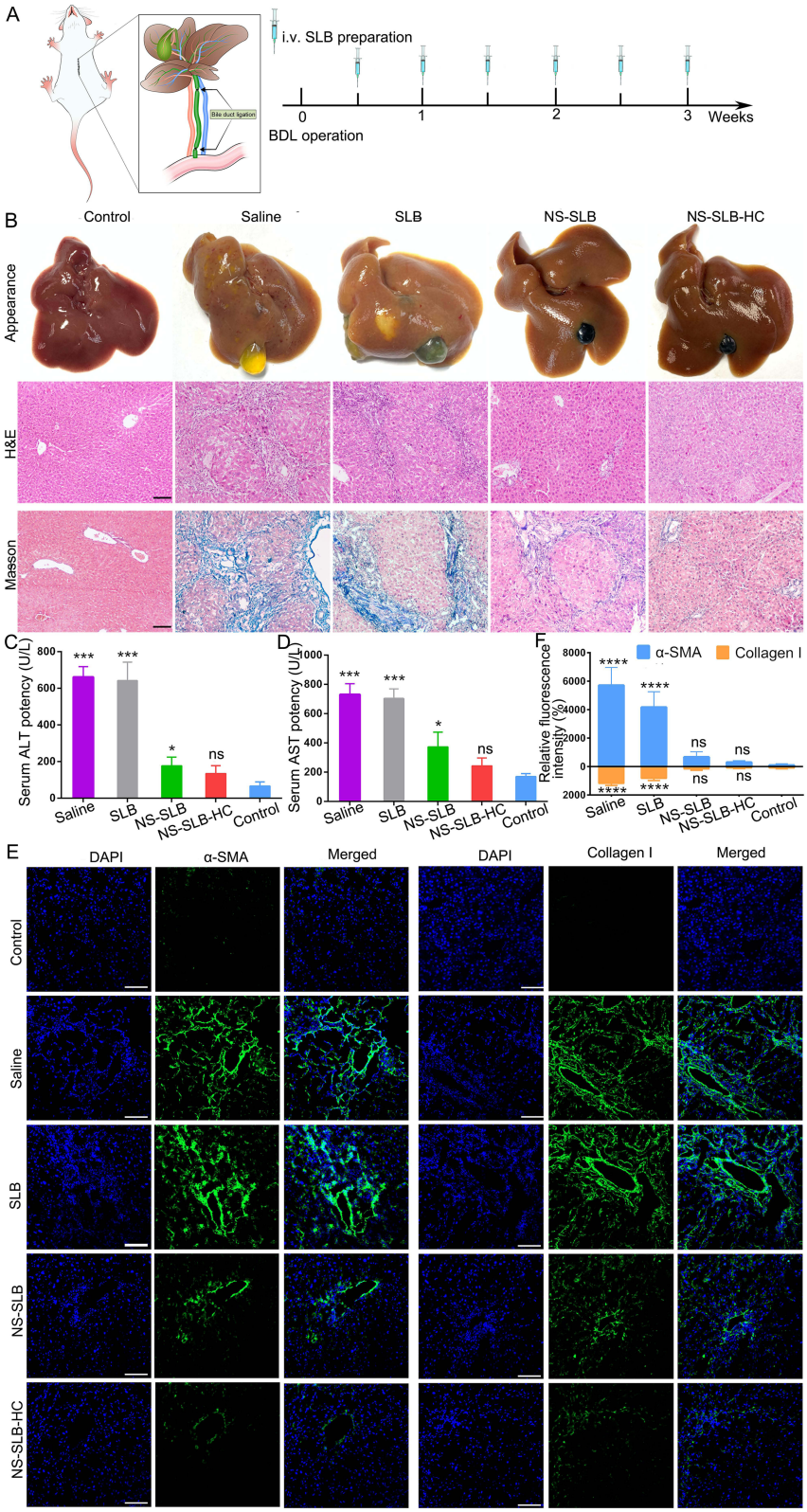

Figure 5 Efficacy of nanosuspensions against bile duct ligation (BDL)-induced hepatic fibrosis in mice. (**A**) Schematic of therapeutic schedule. (**B**) Appearance and histological analysis of liver tissues after 3 weeks of treatment with different formulations. Scale bar, 100 μm. (**C** and **D**) Levels of (C) alanine aminotransferase (ALT) and (D) aspartate aminotransferase (AST) after 3 weeks of treatment. (**E**) Immunofluorescence staining of liver sections against α-smooth muscle actin (α-SMA) or collagen I with Alexa Fluor® 488-labeled IgG (green) after 3 weeks of treatment. Cell nuclei were stained with DAPI (blue). Scale bar, 50 μm. (**F**) Semi-quantitative analysis of immunofluorescence images. Normal mice were used as controls. Data are shown as mean ± SD (n = 5). ****$P < 0.0001$; ***$P < 0.001$; *$P < 0.05$; ns, non-significant difference vs control.

significantly impact the interactions of nanomaterials with biological systems. Previous reports have shown that when particles are larger than 500 nm, macrophages end to clear them via phagocytosis.[41] In contrast, particles with smaller sizes can escape the mononuclear phagocyte system, penetrate the Disse space, and accumulate at the lesion site.

SLB loading rates reach 60%, which are significantly higher than the approximately 7% reported before.[3] Although the previously published system showed satisfactory CD44 targeting and efficacy against hepatic fibrosis, the limited drug loading capacity and substantial carrier material volume may pose challenges for industrial scale-up and raise safety concerns.

The amphiphilic anticancer drug, irinotecan, which has already been approved by the US Food and Drug Administration, can be loaded into carriers at a significantly higher efficiency of 50%.[42] It can also be co-loaded with indocyanine green to enable photothermal therapy.[22] Another amphiphilic anticancer drug, mitoxantrone, has been loaded at an efficiency of 56% into a photosensitizing delivery system.[23] However, both of these systems have a major drawback that the anticancer drugs show appreciable toxicity against healthy tissues,[42,43] which restricts their clinical application. Therefore, these amphiphilic compounds, despite their surfactant-like properties, may be unsuitable for non-oncology drug delivery systems. In contrast, SLB and SLB-M have been associated with a low risk of toxicity and adverse reactions.[25] Consistent with previous work, we found that amphiphilic SLB-M exhibited negligible systemic toxicity during a 3-week treatment. In fact, SLB-M appeared to protect organs from damage, which may be due to the anti-inflammatory properties of SLB or SLB-M. Therefore, SLB-M may be an appropriate carrier for safe drug delivery systems against various diseases.

Conclusions

In this study, we have demonstrated that SLB-M can serve as an effective surfactant for preparing hydrophobic drug delivery systems. Unlike traditional surfactants, when employed as a medical excipient analogue, SLB-M exhibits the ability to establish stronger interactions with hydrophobic molecules through π–π stacking interactions, thereby enhancing its resilience against material-induced hazards. With its multifaceted attributes, the integration of SLB-M could bring intriguing dimensions when combined with other complex hydrophobic drugs.[12] Also, it was reported that nanoparticles ranging in size from 30 to 200 nm preferentially accumulate in tumor tissues.[44,45] Thus, utilizing drug salts as surfactants could lead to innovative nanoformulations for delivering hydrophobic drugs targeted against a wide range of cancers. Additionally, this approach may offer new possibilities for SLB, SLB-M, and other phytomedicine extracts or derivatives to serve as medicine excipient homologues in the design of drug delivery systems.

Acknowledgment

This work was financially supported by the National Natural Science Foundation of China (81872804, 81690261), Nanchong Municipal University Cooperative Scientific Research Project (19SXHZ0445, 19SXHZ0346), and North Sichuan Medical College Doctoral Research Project (CBY19-QD06). We would like to express our gratitude to the Analytical & Testing Center of Sichuan University for their assistance with TEM characterization.

Disclosure

The authors declare no conflicts of interest in this work.

References

1. Bartneck M, Schlosser CT, Barz M, et al. Immunomodulatory therapy of inflammatory liver disease using selectin-binding glycopolymers. *Acs Nano*. 2017;11(10):9689–9700. doi:10.1021/acsnano.7b04630
2. Wang Y, Xiong L, Dong Z, et al. Autophagy-Interfering Nanoboat Drifting along CD44-Golgi-ER Flow as RNAi Therapeutics for Hepatic Fibrosis. *ACS Appl Mater Interfaces*. 2023;15(24):28941–28953. doi:10.1021/acsami.3c03416
3. Li W, Zhou C, Fu Y, et al. Targeted delivery of hyaluronic acid nanomicelles to hepatic stellate cells in hepatic fibrosis rats. *Acta Pharm Sin B*. 2020;10(4):693–710. doi:10.1016/j.apsb.2019.07.003
4. Yang YM, Noureddin M, Liu C, et al. Hyaluronan synthase 2-mediated hyaluronan production mediates Notch1 activation and liver fibrosis. *Sci Transl Med*. 2019;11(496):496. doi:10.1126/scitranslmed.aat9284
5. Tsuchida T, Friedman SL. Mechanisms of hepatic stellate cell activation. *Nat Rev Gastroenterol Hepatol*. 2017;14(7):397–411. doi:10.1038/nrgastro.2017.38

6. Luo J, Zhang P, Zhao T, et al. Golgi apparatus-targeted chondroitin-modified nanomicelles suppress hepatic stellate cell activation for the management of liver fibrosis. *ACS Nano*. 2019;13(4):3910–3923. doi:10.1021/acsnano.8b06924
7. Li R, Zhang J, Liu Q, et al. CREKA-modified liposomes target activated hepatic stellate cells to alleviate liver fibrosis by inhibiting collagen synthesis and angiogenesis. *Acta Biomater*. 2023;168:484–496. doi:10.1016/j.actbio.2023.06.032
8. Warren A, Bertolino P, Benseler V, Fraser R, McCaughan GW, Le Couteur DG. Marked changes of the hepatic sinusoid in a transgenic mouse model of acute immune-mediated hepatitis. *J Hepatol*. 2007;46(2):239–246. doi:10.1016/j.jhep.2006.08.022
9. Trautwein C, Friedman SL, Schuppan D, Pinzani M. Hepatic fibrosis: concept to treatment. *J Hepatol*. 2015;62(1 Suppl):S15–24. doi:10.1016/j.jhep.2015.02.039
10. Fan QQ, Zhang CL, Qiao JB, et al. Extracellular matrix-penetrating nanodrill micelles for liver fibrosis therapy. *Biomaterials*. 2020;230:119616. doi:10.1016/j.biomaterials.2019.119616
11. Di Costanzo A, Angelico R. Formulation strategies for enhancing the bioavailability of silymarin: the state of the art. *Molecules*. 2019;24(11):2155. doi:10.3390/molecules24112155
12. Huo M, Wang H, Zhang Y, et al. Co-delivery of silybin and paclitaxel by dextran-based nanoparticles for effective anti-tumor treatment through chemotherapy sensitization and microenvironment modulation. *J Controlled Release*. 2020;321:198–210. doi:10.1016/j.jconrel.2020.02.017
13. Tan X, Hao Y, Ma N, et al. M6P-modified solid lipid nanoparticles loaded with matrine for the treatment of fibrotic liver. *Drug Deliv*. 2023;30(1):2219432. doi:10.1080/10717544.2023.2219432
14. Elzoheiry A, Ayad E, Omar N, Elbakry K, and Hyder A. Anti-liver fibrosis activity of curcumin/chitosan-coated green silver nanoparticles. *Sci Rep*. 2022;12(1):18403. doi:10.1038/s41598-022-23276-9
15. Etter EL, Mei KC, Nguyen J. Delivering more for less: nanosized, minimal-carrier and pharmacoactive drug delivery systems. *Adv Drug Deliv Rev*. 2021;179:113994. doi:10.1016/j.addr.2021.113994
16. Soliman KA, Ullah K, Shah A, Jones DS, and Singh TRR. Poloxamer-based in situ gelling thermoresponsive systems for ocular drug delivery applications. *Drug Discov Today*. 2019;24(8):1575–1586. doi:10.1016/j.drudis.2019.05.036
17. Wei WB, Bai F, Fan HY. Surfactant-assisted cooperative self-assembly of nanoparticles into active nanostructures. *Iscience*. 2019;11:272–293. doi:10.1016/j.isci.2018.12.025
18. Falconer RJ. Advances in liquid formulations of parenteral therapeutic proteins. *Biotechnol Adv*. 2019;37(7):107412. doi:10.1016/j.biotechadv.2019.06.011
19. Chung JY, Ko JH, Lee YJ, Choi HS, and Kim YH. Surfactant-free solubilization and systemic delivery of anti-cancer drug using low molecular weight methylcellulose. *J Controlled Release*. 2018;276:42–49. doi:10.1016/j.jconrel.2018.02.028
20. Chang Y, Jiao Y, Symons HE, Xu JF, Faul CFJ, Zhang X. Molecular engineering of polymeric supra-amphiphiles. *Chem Soc Rev*. 2019;48(4):989–1003. doi:10.1039/C8CS00806J
21. Chen JX, Wang HY, Li C, Han K, Zhang XZ, and Zhuo RX. Construction of surfactant-like tetra-tail amphiphilic peptide with RGD ligand for encapsulation of porphyrin for photodynamic therapy. *Biomaterials*. 2011;32(6):1678–1684. doi:10.1016/j.biomaterials.2010.10.047
22. Hu S, Dong C, Wang J, et al. Assemblies of indocyanine green and chemotherapeutic drug to cure established tumors by synergistic chemo-photo therapy. *J Controlled Release*. 2020;324:250–259. doi:10.1016/j.jconrel.2020.05.018
23. Wang ZM, Sun MC, Liu T, et al. A surfactant-like chemotherapeutic agent as a nanocarrier for delivering photosensitizers against cancer: a facile drug-delivering-drug strategy. *Int J Pharmaceut*. 2019;562:313–320. doi:10.1016/j.ijpharm.2019.03.037
24. Cheung CW, Gibbons N, Johnson DW, Nicol DL. Silibinin–a promising new treatment for cancer. *Anticancer Agents Med Chem*. 2010;10(3):186–195. doi:10.2174/1871520611009030186
25. Takke A, Shende P. Nanotherapeutic silibinin: an insight of phytomedicine in healthcare reformation. *Nanomedicine*. 2019;21:102057. doi:10.1016/j.nano.2019.102057
26. Bijak M. Silybin, a major bioactive component of milk thistle (silybum marianum L. Gaernt.)-chemistry, bioavailability, and metabolism. *Molecules*. 2017;22(11):1942. doi:10.3390/molecules22111942
27. Ezhilarasan D, Evraerts J, Sid B, et al. Silibinin induces hepatic stellate cell cycle arrest via enhancing p53/p27 and inhibiting Akt downstream signaling protein expression. *Hepatobiliary Pancreat Dis Int*. 2017;16(1):80–87. doi:10.1016/S1499-3872(16)60166-2
28. Qiao JB, Fan QQ, Xing L, et al. Vitamin A-decorated biocompatible micelles for chemogene therapy of liver fibrosis. *J Controlled Release*. 2018;283:113–125. doi:10.1016/j.jconrel.2018.05.032
29. Troeger JS, Mederacke I, Gwak GY, et al. Deactivation of hepatic stellate cells during liver fibrosis resolution in mice. *Gastroenterology*. 2012;143(4):1073–1083.e1022. doi:10.1053/j.gastro.2012.06.036
30. Choi KM, Jang M, Kim JH, Ahn HJ. Tumor-specific delivery of siRNA using supramolecular assembly of hyaluronic acid nanoparticles and 2b RNA-binding protein/siRNA complexes. *Biomaterials*. 2014;35(25):7121–7132. doi:10.1016/j.biomaterials.2014.04.096
31. Csupor D, Csorba A, Hohmann J. Recent advances in the analysis of flavonolignans of Silybum marianum. *J Pharm Biomed Anal*. 2016;130:301–317. doi:10.1016/j.jpba.2016.05.034
32. Zheng J, Ma LT, Ren QY, et al. The influence of astragalus polysaccharide and beta-elemene on LX-2 cell growth, apoptosis and activation. *BMC Gastroenterol*. 2014;14():224. doi:10.1186/s12876-014-0224-8
33. Schinagl M, Tomin T, Gindlhuber J, et al. Proteomic changes of activated hepatic stellate cells. *Int J Mol Sci*. 2021;22(23):12782. doi:10.3390/ijms222312782
34. Shen C, Huang XY, Geng CA, et al. Cytotoxic sesquiterpenoids against hepatic stellate cell line LX2 from Artemisia lavandulaefolia. *Bioorg Chem*. 2020;103:104107. doi:10.1016/j.bioorg.2020.104107
35. Qu C, Zheng D, Li S, et al. Tyrosine kinase SYK is a potential therapeutic target for liver fibrosis. *Hepatology*. 2018;68(3):1125–1139. doi:10.1002/hep.29881
36. Greuter T, Shah VH. Too stiff, too late. Timing is everything in antiangiogenic treatment of liver fibrosis. *Hepatology*. 2019;69(1):449–451. doi:10.1002/hep.30124
37. Chang J, Lan T, Li C, et al. Activation of Slit2-Robo1 signaling promotes liver fibrosis. *J Hepatol*. 2015;63(6):1413–1420. doi:10.1016/j.jhep.2015.07.033
38. Bates J, Vijayakumar A, Ghoshal S, et al. Acetyl-CoA carboxylase inhibition disrupts metabolic reprogramming during hepatic stellate cell activation. *J Hepatol*. 2020;73(4):896–905. doi:10.1016/j.jhep.2020.04.037
39. Chen Y, Chen L, Yang T. Silymarin nanoliposomes attenuate renal injury on diabetic nephropathy rats via co-suppressing TGF-beta/Smad and JAK2/STAT3/SOCS1 pathway. *Life Sci*. 2021;271:119197. doi:10.1016/j.lfs.2021.119197

40. Hu Q, Liu M, You Y, et al. Dual inhibition of reactive oxygen species and spleen tyrosine kinase as a therapeutic strategy in liver fibrosis. *Free Radic Biol Med*. 2021;175:193–205. doi:10.1016/j.freeradbiomed.2021.08.241
41. Nagai N, Ogata F, Ishii M, et al. Involvement of endocytosis in the transdermal penetration mechanism of ketoprofen nanoparticles. *Int J Mol Sci*. 2018;19(7):2138. doi:10.3390/ijms19072138
42. Hu SQ, Lee E, Wang C, et al. Amphiphilic drugs as surfactants to fabricate excipient-free stable nanodispersions of hydrophobic drugs for cancer chemotherapy. *J Control Release*. 2015;220:175–179. doi:10.1016/j.jconrel.2015.10.031
43. Wu J, Waxman DJ. Immunogenic chemotherapy: dose and schedule dependence and combination with immunotherapy. *Cancer Lett*. 2018;419:210–221. doi:10.1016/j.canlet.2018.01.050
44. Makhani EY, Zhang A, Haun JB. Quantifying and controlling bond multivalency for advanced nanoparticle targeting to cells. *Nano Converg*. 2021;8():38. doi:10.1186/s40580-021-00288-1
45. Ikeda-Imafuku M, Wang LL, Rodrigues D, Shaha S, Zhao Z, Mitragotri S. Strategies to improve the EPR effect: a mechanistic perspective and clinical translation. *J Control Release*. 2022;345:512–536. doi:10.1016/j.jconrel.2022.03.043